# Noninvasive Methods for Quantitating Blood Time-Activity Curves from Mouse PET Images Obtained with Fluorine-18-Fluorodeoxyglucose

Leeta A. Green, Sanjiv S. Gambhir, Ashok Srinivasan, Pranab K. Banerjee, Carl K. Hoh, Simon R. Cherry, Susan Sharfstein, Jorge R. Barrio, Harvey R. Herschman and Michael E. Phelps

*Crump Institute for Biological Imaging; Division of Nuclear Medicine, Department of Molecular and Medical Pharmacology; Department of Biomathematics; and Molecular Biology Institute; University of California at Los Angeles School of Medicine, Los Angeles, California*

The mouse model is currently being explored for various applications with PET imaging. Low resolution of current animal scanners relative to mouse size leads to difficulty in quantitating data from mouse PET images. We have, therefore, investigated methods for determining blood time-activity curves (TACs) from mouse PET studies done with fluorine-18-fluorodeoxyglucose (FDG). **Methods:** Eight mice were fasted, the tail vein was injected with 150–300 μCi of FDG and dynamic images were acquired with a CTI/Siemens (Knoxville, TN) animal tomograph for 64.5 min. Concurrently, 11–14 left ventricle (LV) blood samples were drawn directly from the LV chamber. Organ TACs were obtained by drawing circular regions of interest (ROIs) of various sizes on images of the heart, liver and brain. For each mouse, the FDG model parameter $K = (K_1 \times k_3)/(k_2 + k_3)$ was estimated by a Patlak algorithm with various estimates of the blood TAC and, as a reference tissue TAC, the brain TAC. **Results:** Most partial-volume-corrected heart ROI TACs overestimated the LV samples. Blood TACs from heart images produced statistically different estimates of K than did the LV samples. The liver image-derived blood TACs yielded estimates of K that were comparable to those yielded by the LV samples. Estimates of K determined with two directly sampled LV points in conjunction with the liver image-derived TAC were not statistically different from the estimates obtained with the LV samples. The size and location of ROIs on images of the liver minimally affected the TACs. **Conclusion:** We have shown that it is experimentally possible to obtain a blood TAC from mouse studies by repeatedly sampling from the LV. We have also shown that images of the liver can be used to reliably estimate the blood TAC. Future FDG PET studies with the mouse model will benefit from this demonstrated ability to noninvasively quantitate blood TACs directly from FDG PET images.

**Key Words:** fluorine-18-fluorodeoxyglucose; blood time-activity curves; mice; PET; quantitation

**J Nucl Med 1998; 39:729–734**

PET, as well as other in vivo imaging techniques, are increasingly being used with mouse and/or rat models (e.g., in monitoring gene expression with 8-[$^{18}$F]fluoroacyclovir or $^{131}$I-labeled 2′-fluoro-2′-deoxy-1-β-D-arabinofuranosyl-5-iodouracil (*1,2*) and in monitoring tumor growth with fluorine-18-fluorodeoxyglucose (FDG) (*3,4*)). The mouse has been the preferred animal model for many in vivo molecular biology and genetic studies (*5*); hence, many experimental techniques have been developed with mice. For example, transgenic mice can be raised in the laboratory, thus allowing for in vivo genetic studies (*6,7*); human tumors can be ideally studied by xenografting them into athymic mice (*3,4*).

Because rats are significantly larger than mice (the weight of a rat is approximately 10 times that of a mouse), PET images of rats are better able to resolve adjacent structures than those of mice. However, only limited research with transgenic rats has been conducted to date (*8,9*). Furthermore, the model for implanting human tumors into rats has been used only rarely (*10,11*). Additional advantages of using mice include their low cost, easy handling and fast reproductive cycle. Therefore, the mouse model currently has greater applications in genetic and xenograft tumor studies than does the rat model.

Dynamic PET studies are used in conjunction with well-validated tracer kinetic models to obtain estimates of biochemical and physiological parameters. For example, the FDG model parameter $K = (K_1 \times k_3)/(k_2 + k_3)$ is linearly related to the local glucose metabolic rate (*12–14*). Accurate blood and tissue time-activity curves (TACs) are required for estimation of the model parameters. To date, rigorous validation of noninvasive methods to determine blood TACs from mouse FDG-PET studies (as well as for other PET tracers) has not been conducted. Kallinowski et al. (*3*) imaged mice with PET and used arterial catheters in two *nu/nu* mice to obtain blood TACs; they correlated these values with image-derived blood TACs. Hawkins et al. (*4*) imaged *nu/nu* mice with an animal PET system and relied on the noninvasive blood TAC correlation of Kallinowski et al. (*3*) and on limited retro-orbital blood samples. These and other methods of direct blood sampling of mice are technically difficult because of the relatively small diameters of the mouse blood vessels; furthermore, the total blood volume of a mouse is only ~1.7 ml (*15*), making repeated blood sampling physiologically challenging to the mice.

In large animals and humans, blood TACs can be invasively derived by direct arterial sampling or noninvasively derived by drawing regions of interest (ROIs) on PET images of the myocardial left ventricle (LV) (*16,17*). Because of the limited resolution of current PET scanners relative to the size of mice, however, the LV chamber cannot be distinguished from the myocardial tissue on mouse images. ROIs drawn on the heart thus represent activity from the LV and from the myocardium. If the mice are fasted, the myocardium should use fatty acids as its major energy source and thus show suppressed glucose (and therefore FDG) uptake (*18*). Nonetheless, myocardial activity, although reduced, may contribute to the observed heart ROI signal. The kinetics of FDG in the liver, on the other hand, are such that FDG is rapidly cleared from liver tissue (*19–21*). We therefore hypothesized that we could obtain an adequate estimate of the blood TAC from mouse liver images.

Received Feb. 25, 1997; revision accepted Jun. 12, 1997.

For correspondence or reprints contact: Sanjiv S. Gambhir, MD, PhD, Crump Institute for Biological Imaging, UCLA School of Medicine, A-222B CIBI, 700 Westwood Plaza, Los Angeles, CA 90095-1770.

We undertook to develop and validate a method to determine noninvasively blood TACs from mouse FDG-PET studies. We compared direct LV blood sampling from mice and PET image ROI-derived blood TACs, considering liver and heart images. For the former method, we also studied ROI placement effects. Fitting of K in the FDG model (*22*) served as a reference against which to compare various blood curves.

## THEORY

As a consequence of the partial-volume effect (*23*), measured image counts for small objects (relative to scanner resolution) represent only a fraction of the true counts in the region. This fraction, called the recovery coefficient (RC) ranges between 0 and 1. Further error is introduced to the measurement by experimental fluctuations, and we assume this error to be Gaussian error, e(t). Equation 1 describes these consequences:

$$\text{observed counts} = RC \times (\text{true counts}) + e(t). \quad \text{Eq. 1}$$

Because of region inhomogeneity and the spillover effect, the true average counts in a region often are the weighted sum of multiple activities. For example, the true liver ROI counts, C(t), are composed of the pure blood TAC, B(t), liver tissue TAC, T(t) and spillover of activity from neighboring areas, S(t), as given by Equation 2:

$$C(t) = c \times B(t) + (1 - c) \times T(t) + S(t). \quad \text{Eq. 2}$$

Here, c is a coefficient between 0 and 1; c and (1 − c) represent the fractions of activity in the ROI that are contributed by vasculature and liver tissue, respectively. The measured counts, L(t), are given in Equation 3 and Equation 4 and follow directly from Equations 1 and 2:

$$L(t) = RC_{Liver} \times C(t) + e(t) \quad \text{Eq. 3}$$

$$L(t) = RC_{Liver}[c \times B(t) + (1 - c) \times T(t) + S(t)] + e(t). \quad \text{Eq. 4}$$

$RC_{Liver}$ is a recovery coefficient that accounts for the liver partial-volume effect (*23*). In this study, we develop and validate a model to determine an estimate of B(t) from the known information, L(t).

According to the model of Choi et al. (*19*) for FDG in human normal liver tissue, T(t) can be expressed as

$$T(t) = f(K_1, k_2, k_3, k_4) \otimes B(t + TD), \quad \text{Eq. 5}$$

where $f(K_1, k_2, k_3, k_4)$ is a function of the usual FDG model parameters (*12,13*), TD represents a time delay and ⊗ denotes the mathematical convolution operation. If it is assumed that this model extends to mice, Equations 4 and 5 give

$$L(t) = RC_{Liver}\{c \times B(t) + (1 - c) \times [f(K_1, k_2, k_3, k_4) \otimes B(t + TD)] + S(t)\} + e(t). \quad \text{Eq. 6}$$

Because there are unidentifiable parameters in this model, we have explored a simplified model. Suppose the terms in the braces can be approximated as U(t) × B(t) for some function, U(t). Then, Equation 6 can be reduced to

$$L(t) \sim RC_{Liver}[U(t) \times B(t)] + e(t), \quad \text{Eq. 7}$$

which can be further simplified to

$$L(t) \sim RC_{Liver}[u \times B(t)] + e(t) \quad \text{Eq. 8}$$

if U(t) equals some constant, u, for all time. Equation 8 is the model that we validate below; this model describes how to estimate B(t) from the liver image ROI TAC. Below we describe how the product $u_L = RC_{Liver} \times u$ is estimated.

The heart image ROI TAC was also explored as a possible estimate for B(t). Let M(t) denote the true dynamic counts in a myocardial ROI. Because of resolution constraints, the LV chamber cannot be distinguished from the myocardial tissue. Although ROI sizes (see below) were small enough to fit within the LV chamber, we could not visually determine whether any myocardial tissue was enclosed in the ROI. The equation used to explain M(t) is

$$M(t) = w \times LV(t) + (1 - w) \times Mt(t) + So(t), \quad \text{Eq. 9}$$

where Mt(t) is the myocardial tissue TAC, LV(t) is the activity in the LV over time, So(t) accounts for spillover and w is a coefficient between 0 and 1; w and (1 − w) represent the fractions of the ROI that contain the LV chamber and myocardial tissue, respectively. Let $RC_{Myocardial}$ reflect the myocardial partial-volume effect. From Equations 1 and 9, the observed ROI counts, Mo(t), are thus given by Equation 10:

$$Mo(t) = RC_{Myocardial}[w \times LV(t) + (1 - w) \times Mt(t) + So(t)] + e(t). \quad \text{Eq. 10}$$

Activity in the LV is the blood TAC, so LV(t) = B(t). If myocardial glucose utilization is sufficiently suppressed, there is no significant uptake by myocardial tissue, and Mt(t) ~ 0. If it is assumed that So(t) is negligible, then Mo(t) is approximately linearly related to the blood TAC (Eq. 11):

$$Mo(t) \sim RC_{Myocardial}[w \times B(t)] + e(t). \quad \text{Eq. 11}$$

Below we describe how the product $w_M = RC_{Myocardial} \times w$ is estimated.

## MATERIALS AND METHODS

### General Strategy

Three general strategies were used to estimate the coefficients in Equations 8 and 11. The first strategy arrived at estimates of $RC_{Liver}$ and $RC_{Myocardial}$ by consideration of the geometry of the liver and the heart. The other two strategies involved comparing PET image-derived TACs to TACs derived from direct LV blood sampling. The details of these three different approaches are described below. Table 1 provides a summary of the notation used in this article for the different estimates of $RC_{Liver}$, $RC_{Myocardial}$, $u_L$ and $w_M$. Note that the subscript M refers to the myocardial LV chamber. The subscript LV is not used because subscripts beginning with L have been reserved for the liver.

### Anatomical Measurements

Three mice were anesthetized, killed and sectioned (50–200 μm) with a PMV (PMV Inc., Knoxville, TN) cryostat by a previously described method (*24*). From the coronal cross sections, estimates of LV chamber size and liver size were obtained in two dimensions. Measurements were recorded for several sections and averaged. Estimates for the sizes in the third dimension were obtained by noting the number and thickness of the slices needed to cut through the entire liver or LV chamber. For the liver, the sizes of the left and right lobes were recorded in this dimension. The sizes in each dimension were averaged across the three mice to obtain a mean size estimate. The mean size estimate was then used to obtain geometric recovery coefficients, $RC_M$ and $RC_L$, for partial-volume correction for the LV chamber and liver, respectively. The estimates for the geometric recovery coefficients were based on a one-dimensional bar phantom approximation obtained by use of the estimated effective in-plane and axial FWHM for the scanner (*25*) and the average diameter of the ROI.

**TABLE 1**
Notation for Estimates of Model Parameters

| Symbol | Method of estimation | What is being estimated |
|---|---|---|
| $RC_L$ | Based on geometry of liver | $RC_{Liver}$ |
| $RC_M$ | Based on geometry of LV | $RC_{Myocardial}$ |
| $u_{L\_AM}$ | All mice were used in one least squares fit of liver image TACs to LV samples | $RC_{Liver} \times u$ |
| $w_{M\_AM}$ | All mice were used in one least squares fit of heart image TACs to LV samples | $RC_{Myocardial} \times w$ |
| $u_{L\_MS}$ | Mouse-specific ratio for liver image TACs | $RC_{Liver} \times u$ |
| $w_{M\_MS}$ | Mouse-specific ratio for heart image TACs | $RC_{Myocardial} \times w$ |

LV = left ventricle; TACs = time-activity curves.

### Preparation of FDG

FDG was synthesized by the method described by Hamacher et al. (*26*). The radiochemical purity was >99%. The specific activity was ~5 Ci/$\mu$mol.

### Animal Preparations and Positioning

Nineteen C3H/HeN mice were fasted (but allowed to drink) for 6–12 hr before imaging and were anesthetized with ~0.8 ml of 2.5% tribromoethanol (Avertin) injected intraperitoneally (i.p.). The mice were immediately placed in the supine position on a piece of cardboard, and their limbs were strapped down with rubber bands. FDG (150–300 $\mu$Ci in 0.2 ml saline) was injected via the tail vein, and then ~0.2 ml of saline was injected. The mice were positioned in the scanner such that the long axis of the scanner was perpendicular to the sagittal planes of the mice.

### Image Acquisition

The mice were imaged with a CTI/Siemens animal tomograph [model 713; (Siemens, Knoxville, TN)], which collects 15 planes separated by 3.38 mm (*27*). To correct for photon attenuation, a 10–20-min transmission scan was acquired for each mouse before FDG injection. Immediately after the injection of FDG, 17 emission scans were obtained over a total of 64.5 min. The following sequence was used: nine 30-sec, four 5-min and four 10-min scans. The data were reconstructed with a Shepp-Logan filter with a cutoff frequency of 0.5 to give an effective in-plane resolution of ~4 mm and an axial resolution of ~4.6 mm.

### LV Blood Sampling

During acquisition of the emission images, 11–14 blood samples were drawn directly from the LV (*28*) with a 1-cc U-100 insulin syringe connected to a 28.5-gauge needle (frequency, four or five samples in the first 4 min, three to six samples in the next 16–17 min and three to five samples in the remaining 43–44 min). All whole-blood samples were weighed (minimum weight, ~1 mg; maximum weight, ~40 mg), and their FDG activity was measured in a cylinder-well counter. Units were calibrated from counts per milligram per second to counts per pixel per second, with the assumption of a blood density of 1 g/ml and with a correction factor obtained in a manner similar to that of Choi et al. (*19*), with the exceptions that a small cylinder (~6 cm in diameter) filled with ~278 $\mu$Ci of FDG was scanned for 5 min and two 0.025-ml aliquots were drawn. Activity from the aliquots (determined with the well counter) was compared with image counts. Three raw datasets were examined: (a) LV blood samples weighing 15 mg or less were ignored, leaving an average of 8 samples per mouse (range, 4–10); (b) LV blood samples weighing 10 mg or less were ignored, leaving an average of 10 or 11 samples per mouse (range, 7–12); and (c) no data were ignored, regardless of the sample volume.

LV TACs for each mouse were generated from each dataset as follows. Raw LV data were linearly interpolated to the endpoints of the scan times. The value at time zero was explicitly set to zero. For any scan interval that included at least one LV sample, all the values in that interval and the (linearly interpolated) endpoints were used to calculate the integral of activity over that time interval. This integral was then divided by the length of the time interval, and the resulting value was recorded at the middle time point of the interval. These data are referred to here as LV samples and were used in estimating $w_{M\_AM}$ and $u_{L\_AM}$ (defined below; Table 1) and in estimating the FDG model parameter K.

### Analysis of Data

The dynamic sagittal image data were resliced into 32 dynamic coronal sections with the Crump Institute Integrated Imaging Software Package written in the IDL language (Research Systems, Inc., Boulder, CO) and currently under development in our laboratory. Plane averaging was accomplished during the reslice processing. One ROI (area enclosed, nine square pixels) was drawn centered on the image of the heart during the time frame with heart activity best distinguishable from background, and one was drawn on the brain (13 square pixels) during the last time frame. Four ROIs were drawn on the left lobe of the liver during the time frame with peak liver activity (all four during the same frame but with different frames for different mice, depending on where the liver activity was best distinguishable). The four liver ROIs differed in size and location within the liver, such that three of the ROIs had the same center but different areas (8, 26 and 43 square pixels); the center of the fourth ROI was displaced (so that the ROI still enclosed the peak activity of the left lobe) from the other center by 7–11 pixels, and the area of this ROI was 29 square pixels. All ROIs were drawn on the resliced coronal sections and applied to all times to give TACs derived from heart, brain and liver images in units of counts per pixel per second. (One square pixel equals 0.61 $mm^2$ .)

Areas under the curve (AUCs) were calculated for all TACs. All numerical integration was performed with the int_tabulated routine in IDL, which uses a five-point Newton-Cotes integration method.

For both liver and heart, two methods were explored to obtain estimates for the constant of proportionality between the image-derived TAC and the directly sampled blood data. The methods rely on Equation 8 for the liver and Equation 11 for the heart. In the first method, a global (across all mice) proportionality constant (ratio of image counts to LV samples) was estimated by a least squares fit for both liver ($u_{L\_AM}$) and heart ($w_{M\_AM}$). In the second approach, each mouse was considered individually: for each mouse, a mouse-specific proportionality constant for both liver ($u_{L\_MS}$) and heart ($w_{M\_MS}$) was estimated by averaging the ratio of the image counts to the LV raw data at the times of the last two raw

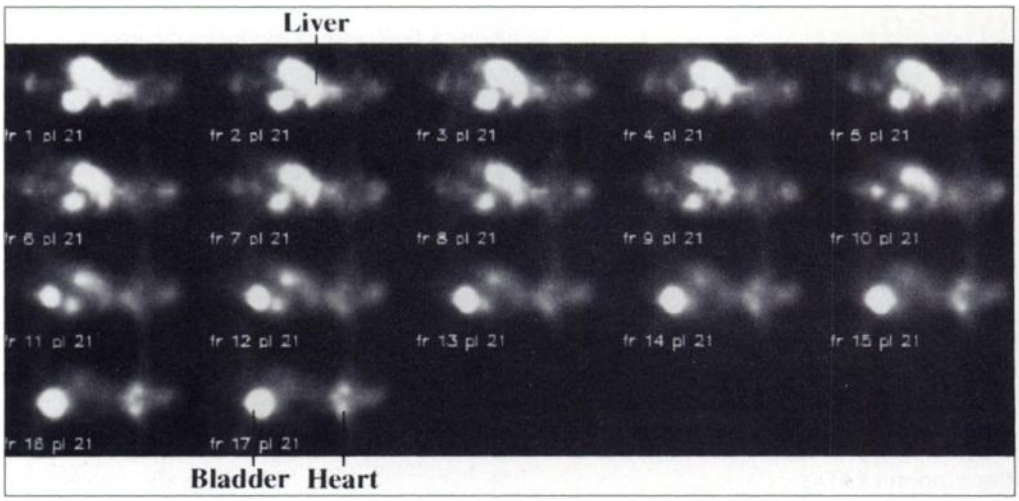


**FIGURE 1.** Dynamic resliced coronal cross-sectional images from typical PET study done with $^{18}$F-FDG at fixed plane. Scaling was done according to global maximum. Time progression, frames (fr) 1–17, is indicated. Early times show FDG uptake in liver. FDG clears through kidneys and bladder. Prominent bladder and myocardial activities can be seen at late times.

LV blood FDG activities. The image counts were linearly interpolated to the times of the last two LV raw data points.

To obtain image-derived blood TACs, the four liver image TACs from each mouse were averaged and divided by $u_{L\_AM}$ or $u_{L\_MS}$, where $u_{L\_AM}$ was averaged over estimates from all four ROIs. Similarly, the heart image TACs were divided by $w_{M\_AM}$, $w_{M\_MS}$ or heart geometric recovery coefficient $RC_M$. The FDG parameter K was estimated by the Patlak algorithm (skipping the first 10 points, which is approximately up to 10 min) (*22*) with the brain image TAC as the reference tissue curve and each of the following as blood TAC: (a) liver image TAC divided by $u_{L\_AM}$; (b) liver image TAC divided by $u_{L\_MS}$; (c) LV samples; (d) heart image TAC divided by $w_{M\_AM}$; (e) heart image TAC divided by $w_{M\_MS}$; and (f) heart image TAC divided by $RC_M$.

A paired Student's t-test was used to test the hypothesis that the estimates for K (as obtained with LV samples versus image-derived blood TAC) are equal (*29*). Analysis of variance (*29*) was used to compare the AUCs of the differently sized and placed liver ROIs (each normalized to the AUC of the corresponding LV samples). All significance levels were set at 0.05.

## RESULTS

The liver measured an average of 10.6 ± 1.2 mm by 12.6 ± 0.38 mm in the coronal plane and 9.9 ± 0.70 (left lobe) mm or 14.7 ± 0.83 mm (right lobe) in the anterior to posterior direction, to give an $RC_L$ of 0.97–0.98. The heart LV chamber measured an average of 5.0 ± 0.17 mm by 6.0 ± 0.84 mm in the coronal plane and 4.6 ± 0.52 mm in the third direction, to give an $RC_M$ of 0.52. (Values are the arithmetic mean ± s.d.)

Eleven of a total of 19 mice were eliminated from the FDG PET study because they had been fasted for fewer than 6 hr or because of experimental complications (e.g., early death or faulty FDG injection). One mouse died during frame 17, and only the first 15 frames (up to 44.5 min postinjection) were included in the study. Internal bleeding, determined by autopsy, was recorded as the cause of death of this mouse. All other mice tolerated the direct LV sampling procedure markedly well.

Figure 1 shows resliced coronal PET images from a typical dynamic study. ROIs drawn on these images were used to obtain TACs. At early times, the liver and abdominal activities were well visualized, whereas at later times, the bladder, brain and sometimes cardiac activities predominated. In many of the fasted mice, inadequate suppression of myocardial tissue uptake of FDG activity was noted.

Table 2 shows the estimates obtained for $u_{L\_AM}$ and $u_{L\_MS}$ when liver ROI TACs were compared with LV samples (generated from the complete dataset). The estimates (mean ± s.e.m.) and ranges of estimates for the proportionality constants are shown. Also shown are the averages (±s.d.) for all mice of the percent difference between K estimated with liver ROI TACs divided by the indicated parameter estimate and with LV samples. Note that the percent difference in the K estimate was about twice as high for $u_{L\_AM}$ as for $u_{L\_MS}$. A p value of > 0.05 indicates that the estimate obtained for K with liver ROI TAC divided by the parameter estimate was not statistically different from the estimate obtained with direct LV samples. Almost identical results were obtained when the modified raw blood datasets were used in the analysis. The only noteworthy difference was that when LV samples 1 (ignoring all blood samples weighing less than 15 mg) was compared with liver ROI TACs divided by $u_{L\_AM}$ (0.58 ± 0.17), the estimates for K were statistically different (p = 0.025). However, relative to K estimates obtained from LV samples 1, K estimates obtained with liver ROI TACs divided by $u_{L\_MS}$ were not statistically different (p = 0.084); the percent difference (13 ± 9) was about twice as high as that obtained with liver ROI TACs divided by $u_{L\_AM}$, as was seen in the complete dataset.

Estimates for heart $w_{M\_AM}$ were all ~0.45 ± 0.2, and the ranges for $w_{M\_MS}$ were all 0.44–2.0. K estimates obtained with heart ROI TACs divided by $RC_M$, $w_{M\_MS}$ or $w_{M\_AM}$ were significantly different from those obtained with LV samples (all p < 0.009; all averaged percent differences > 68%).

Figure 2 shows an example of a comparison of the LV samples with the scaled heart and liver ROI TACs. Myocardial ROI TAC divided by $w_{M\_AM}$ or $RC_M$ (not shown) overestimated LV samples at late times and exhibited an overall shape inconsistent with LV samples and inconsistent across mice (not shown). Liver ROI TACs divided by $u_{L\_AM}$ and $u_{L\_MS}$ both showed good agreement with LV samples.

AUCs of differently sized and placed liver ROIs were not statistically different (p = 0.23); hence, the various liver ROI TACs for each mouse were averaged. The four estimates for

**TABLE 2**
Liver Region-of-Interest Time-Activity Curves Versus LV Samples*

| Parameter | Estimate | % Difference of K | p |
|---|---|---|---|
| $u_{L\_AM}$ | 0.58 ± 0.14† | 17 ± 16‡ | 0.11 |
| $u_{L\_MS}$ | 0.51–0.82 | 9.2 ± 9‡ | 0.34 |
| $RC_L$ | 0.97–0.98 | | |

*The complete raw blood dataset was used to generate the LV samples.
†Arithmetic mean ± s.e.m.
‡Arithmetic mean ± s.d.

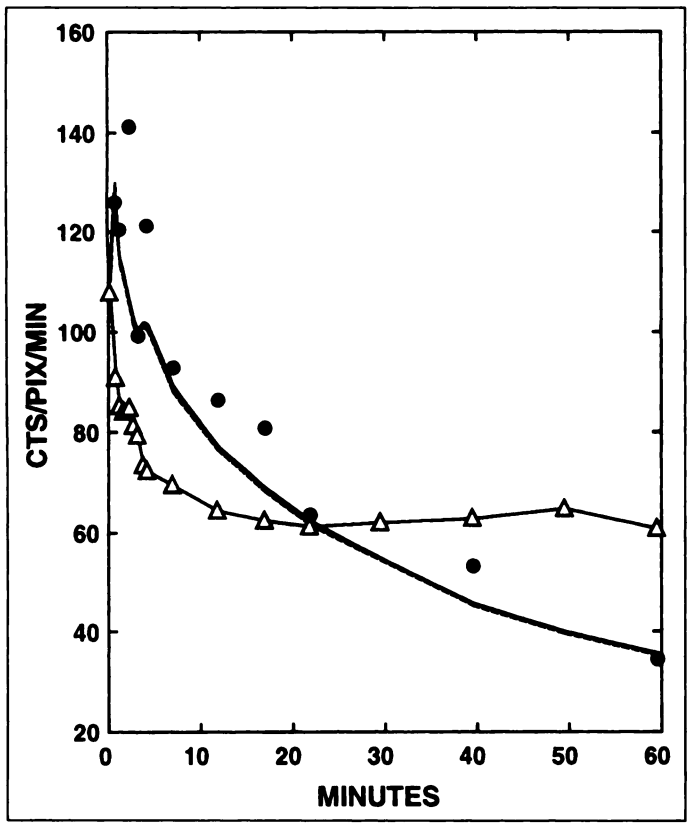


**FIGURE 2.** LV samples and scaled ROI TAC for a typical mouse. LV samples (closed circles) were generated from complete raw data as described in Materials and Methods. Heart ROI TAC was divided by least squares proportionality constant ($w_{M\_AM}$ = 0.45) (open triangles). Heart ROI TAC overestimated LV samples beginning at about 30 min postinjection. Liver ROI TAC was divided by $u_{L\_AM}$ (solid line, no symbol) and $u_{L\_MS}$ (broken line, no symbol) and agreed well with LV samples. CTS/PIX/MIN = counts per pixel per minute.

$u_{L\_AM}$ were all within 6% of each other; therefore, an average of those estimates was used to generate the (averaged) liver ROI TAC-derived blood TAC for estimating K (Table 2).

## DISCUSSION

The liver image TAC provides a good approximation of the direct LV samples, but the heart image TAC provides a poor approximation. The shape of the liver image TAC resembles that of the LV samples, whereas the heart image TAC does not. Future investigators can estimate blood TACs by use of liver ROI TACs divided by either the $u_{L\_AM}$ reported here or by $u_{L\_MS}$ directly determined from two blood samples, depending on the level of accuracy needed (~20% versus ~10%; Table 2). To calculate the local glucose metabolic rate, one blood sample is needed to determine plasma glucose levels; thus, only one additional blood sample is required to obtain $u_{L\_MS}$.

If T(t) and S(t) in Equation 4 are negligible, this equation could be reduced to Equation 8 (with c = u), and the estimate for $u_L$ would be approximately equal to the blood volume fraction of the liver, c, because $RC_L \sim 1$. However, Storey et al. (*30*) have determined the whole-blood fraction of normal mouse liver to be 31%, almost 50% lower than our least squares estimate for $u_L$. This result suggests that T(t) and/or S(t) is not negligible, which could explain the variation between mice. The parameters in Equation 6 for each mouse fluctuate according to the animal's precise metabolic state, and the spillover contribution may depend in part on the rate at which the renal system clears FDG. Nonetheless, FDG PET image liver TACs can be modeled as directly proportional to LV samples (Eq. 8), with proportionality estimated as described above.

We ignored the effect of ROI size and used the average liver ROI size to estimate the recovery coefficient because we observed that estimates obtained for the proportionality constant, $u_L$, with variously sized ROIs were within a few percentages. We found no significant difference among the variously placed liver ROIs, which were drawn on the left lobe of the liver in an attempt to avoid spillover activity from the kidneys. The right kidney sits directly inferior to the right lobe of the liver. The liver image TACs from ROIs within the right lobe of the liver might prove to be significantly different from those within the left lobe.

The heart TAC divided by $w_{M\_AM}$, $w_{M\_MS}$ or $RC_M$ yielded FDG model parameter estimates grossly different from those obtained with LV samples. The heart image ROI TACs had shapes inconsistent with the LV samples shapes resulting in large K discrepancies and a large coefficient of variation (44%) in estimating $w_{M\_AM}$. These observations suggest that the assumptions made in developing model Equation 11 are invalid. Violations occur because of myocardial uptake of FDG and/or spillover from areas neighboring the heart. To minimize the former, the mice were fasted for several hours before FDG injection in the hope that the myocardium would rely on fatty acids and not glucose as its major energy source (*18*). Nonetheless, all but one of the blood TACs from heart images, when corrected for the partial-volume effect or divided by the estimated least squares proportionality constant, overestimated LV samples at late times. (Note that by definition of $w_{M\_MS}$, the heart image TAC divided by $w_{M\_MS}$ will agree with the LV samples at late times.) Various diets and fasting protocols were attempted; none of them led to consistent blood TACs from heart images.

Myocardial tissue activity influenced the observed ROI counts in two ways. First, spillover of tissue activity into the LV chamber contributed to the observed signal. Second, because of resolution constraints, the left ventricle could not be distinguished from the myocardium; therefore, ROIs may have explicitly enclosed myocardial tissue. When the ROIs reside entirely within the LV chamber, spillover myocardial tissue activity can be accounted for by So(t) (Eq. 10) and w = 1 in Equations 10 and 11, so that $w_M$ is reduced to $RC_{Myocardial}$; hence, we studied the effect of dividing the heart ROI TAC by $RC_M$.

Although we were not able to completely suppress myocardial tissue uptake of FDG, other investigators have not reported similar difficulties. Kallinowski et al. (*3*) did not observe blurring between myocardial tissue and LV activities. They reported a regression correlation of 0.93 between the heart image blood TAC and sampled blood TAC for one mouse (*3*). Note, however, that they had direct serial blood samples for only two mice and reported statistics for only one mouse, constituting a small sample size from which to draw kinetic inferences. Furthermore, Kallinowski et al. (*3*) and Hawkins et al. (*4*) both used *nu/nu* mice in their studies, whereas we used C3H/HeN mice. This difference suggests that myocardial uptake of FDG may differ between strains of mice.

Preliminary results showed that almost immediately after injection, the blood TAC decreased very rapidly. To observe this steep decrease, both direct blood samples and image data were acquired with a greater frequency at earlier times during the study than at later times.

There are various methods for sampling blood from mice, including retro-orbital sampling and jugular vein sampling. We chose to sample directly from the LV because it is the most

direct arterial source and least complicated method to accomplish experimentally. Furthermore, intracardiac sampling has been shown to be very safe, with a death rate of less than 5% in newborn mice (*28*). The mice withstood blood sampling remarkably well. Although the total volume drawn from each mouse was about 0.24 ml, we injected about 0.4 ml of fluid into the mice (tracer and saline). Regardless of the method, however, direct blood sampling from mice is subject to experimental error; therefore, the true blood TAC obtained from this sampling is actually subject to statistical variations and is not a gold standard. For example, error is encountered because of the sensitivity of small sample volumes to the accuracy of experimental equipment. To combat this error, we tried ignoring raw blood samples weighing less than 10 mg or 15 mg, criteria chosen based on balance accuracy ($\pm 0.1$ mg) and outliers. Although this strategy yielded fewer data, the s.d. in the parameter estimates decreased because many of the eliminated points were outliers. For both the liver and the heart image TACs, almost identical results were obtained when the complete or modified raw blood datasets were used in the analysis, suggesting that these small samples alone did not significantly affect the results. We further attempted to overcome the effect of experimental error in the raw blood samples by using the integrated values described in Materials and Methods. The integrated values also represented the way in which the image data were recorded.

Human studies have shown that FDG in whole blood and plasma rapidly equilibrates; therefore, whole blood can be used to approximate plasma FDG concentrations (*17*). We assumed that this approximation extends to mice. Because blood samples were too small to reliably isolate plasma, radioactivity in whole-blood samples instead of in plasma samples was counted. The approximation might not hold for other tracers that equilibrate differently.

Preliminary studies revealed that calculations of the calibration coefficient with the well counter versus the scanner varied with aliquot size and cylinder size. The former effect results from the variability of the efficiency of the well counter for different volumes. The latter effect is attributed to scatter differences. Thus, it is worthwhile to calibrate between scanner and well counter with cylinder sizes similar to object sizes and aliquot volumes close to blood sample volumes.

## CONCLUSION

We were able to dynamically image mice with FDG PET and noninvasively determine blood TACs. Estimates for the FDG parameter K with the scaled liver ROI TACs and LV samples were within ~10%–20%. Partial-volume-corrected heart ROI TACs overestimated the directly sampled blood TAC at late times and were therefore unreliable approximations of the LV samples. ROI size and location on images of the left lobe of the liver had a minimal effect on the derived TAC.

The techniques illustrated here can also be used to validate noninvasive determinations of blood TACs for other tracers. In mouse strains for which other tracers have minimal myocardial uptake, the heart ROI TAC might provide the best approximation of directly sampled blood TAC. This would need to be determined experimentally.

## ACKNOWLEDGMENTS

We thank Judy Edwards, Waldemar Ladno, Alan Oshiro, Ron Sumida, Parag Shah, Vaughn Davis and Ali Borghei for technical assistance. This work was partially supported by funding from DOE contract DE-FC03-87ER60615, the DANA Foundation, a Student Fellowship Award from the Education and Research Foundation of the Society of Nuclear Medicine and NIH training grant GM08185-9. An abstract of this paper was presented in the data analysis and instrumentation walking poster session at the 43rd Annual Meeting of the Society of Nuclear Medicine, June 3–5, 1996, Denver, CO.

## REFERENCES

1. Srinivasan A, Gambhir SS, Green AL, et al. A PET reporter gene (PRG)/PET reporter probe (PRP) technology for repeatedly imaging gene expression in living animals [Abstract]. *J Nucl Med* 1996;37(suppl):107P–108P.
2. Tjuvajev J, Finn R, Watanabe K, et al. Noninvasive imaging of herpes virus thymidine kinase gene transfer and expression: a potential method for monitoring gene therapy. *Cancer Res* 1996;56:4087–4095.
3. Kallinowski F, Brownell AL, Vaupel P, Brownell GL. Combined tissue oxygen tension measurement and positron emission tomography studies on glucose utilization in oncogene-transformed cell line tumour xenografts in nude mice. *Br J Radiol* 1991;64:350–359.
4. Hawkins RA, Choi Y, Scates S, et al. An animal model for *in vivo* evaluation of tumor glycolytic rates with positron emission tomography. *J Surg Oncol* 1993;53:104–109.
5. Silver LM. *Mouse genetics: concepts and applications*. New York: Oxford University Press; 1995:12–13.
6. Boyd AL, Samid D. Review: molecular biology of transgenic animals. *J Anim Sci* 1993;3:1–9.
7. Bradley A, Hasty P, Davis A, Ramirez-Solis R. Modifying the mouse: design and desire. *Biotechnology* 1992;10:534–539.
8. Mullins JJ, Mullins LJ. Transgenesis in nonmurine species. *Hypertension* 1993;22: 630–633.
9. Mullins LJ, Mullins JJ. Transgenesis in the rat and larger mammals. *J Clin Invest* 1996;97:1557–1560.
10. Bulte JW, Go KG, Zuiderveen F, The TH, de Leij L. Intracerebral and subcutaneous xenografts of human SCLC in the nude rat: comparison of monoclonal antibody localization and tumor infiltrating lymphocytes. *J Neurooncol* 1993;16:11–18.
11. DiResta GR, Lee J, Larson SM, Arbit E. Characterization of neuroblastoma xenograft in rat flank. I. Growth, interstitial fluid pressure, and interstitial fluid velocity distribution profiles. *Microvasc Res* 1993;46:158–177.
12. Phelps ME, Huang SC, Hoffman EJ, Selin C, Sokoloff L, Kuhl DE. Tomographic measurement of local cerebral glucose metabolic rate in humans with ($^{18}$F)2-fluoro-2-deoxy-D-glucose: validation of method. *Ann Neurol* 1979;6:371–388.
13. Huang SC, Phelps ME, Hoffman EJ, Sideris K, Selin CJ, Kuhl DE. Noninvasive determination of local cerebral metabolic rate of glucose in man. *Am J Physiol* 1980;238:E69–E82.
14. Sokoloff L, Reivich M, Kennedy C, et al. The [$^{14}$C]deoxyglucose method for the measurement of local cerebral glucose utilization: theory, procedure, and normal values in the conscious and anesthetized albino rat. *J Neurochem* 1977;28:897–916.
15. Davies B, Morris T. Physiological parameters in laboratory animals and humans. *Pharm Res* 1993;10:1093–1095.
16. Weinberg IN, Huang SC, Hoffman EJ, et al. Validation of PET-acquired input functions for cardiac studies. *J Nucl Med* 1988;29:241–247.
17. Gambhir SS, Schwaiger M, Huang SC, et al. Simple noninvasive quantification method for measuring myocardial glucose utilization in humans employing positron emission tomography and fluorine-18 deoxyglucose. *J Nucl Med* 1989;30:359–366.
18. Ishiwata K, Ishii K, Sasaki T, et al. Synthesis and preliminary evaluation of [1-$^{11}$C]hexanoate as a PET tracer of fatty acid metabolism. *Ann Nucl Med* 1995;9:51–57.
19. Choi Y, Hawkins RA, Huang SC, et al. Evaluation of the effect of glucose ingestion and kinetic model configurations of FDG in the normal liver. *J Nucl Med* 1994;35: 818–823.
20. Gallagher BM, Fowler JS, Gutterson NI, MacGregor RR, Wan CN, Wolf AP. Metabolic trapping as a principle of radiopharmaceutical design: some factors responsible for the biodistribution of [$^{18}$F]2-deoxy-2-fluoro-D-glucose. *J Nucl Med* 1978;19:1154–1161.
21. Yoshioka T, Takahashi H, Oikawa H, et al. Accumulation of 2-deoxy-2[$^{18}$F]fluoro-D-glucose in human cancers heterotransplanted in nude mice: comparison between histology and glycolytic status. *J Nucl Med* 1994;35:97–103.
22. Patlak CS, Blasberg RG, Fenstermacher JD. Graphical evaluation of blood-to-brain transfer constants from multiple-time uptake data. *J Cereb Blood Flow Metab* 1983;3:1–7.
23. Hoffman EJ, Huang SC, Phelps ME. Quantitation in positron emission computed tomography I. Effects of object size. *J Comput Assist Tomogr* 1979;3:299–308.
24. Larsson B, Ullber S. Whole-body autoradiography. *J Histochem Cytochem* 1981;29: 216–225.
25. Gambhir SS. *Quantitation of the physical factors affecting the tracer kinetic modeling of cardiac positron emission tomography data* [PhD thesis]. Los Angeles; University of California; 1990.
26. Hamacher K, Coenen HH, Stocklin G. Efficient stereospecific synthesis of no-carrier-added 2[$^{18}$F]-fluoro-2-deoxy-D-glucose using amino polyether supported nucleophilic substitution. *J Nucl Med* 1986;27:235–238.
27. Cutler D, Cherry SR, Hoffman E, Digby W, Phelps M. Design features and performance of a PET system for animal research. *J Nucl Med* 1992;33:595–604.
28. Grazer, FM. Technic for intravascular injection and bleeding of newborn rats and mice. *Proc Soc Exp Biol Med* 1958;99:407–409.
29. Ross S. *Introduction to probability and statistics for engineers and scientists*. New York: John Wiley and Sons; 1987:226–227,306–316.
30. Storey RH, Wish L, Furth J. Organ erythrocyte and plasma volumes of tumor-bearing mice: the oligemia of neoplasms. *Cancer Res* 1951;11:943–947.